
Biologically Inspired Dynamic Textures for Probing Motion Perception

Jonathan Vacher
CNRS UNIC and Ceremade
Univ. Paris-Dauphine
75775 Paris Cedex 16, FRANCE
vacher@ceremade.dauphine.fr

Andrew Isaac Meso
Institut de Neurosciences de la Timone
UMR 7289 CNRS/Aix-Marseille Université
13385 Marseille Cedex 05, FRANCE
andrew.meso@univ-amu.fr

Laurent Perrinet
Institut de Neurosciences de la Timone
UMR 7289 CNRS/Aix-Marseille Université
13385 Marseille Cedex 05, FRANCE
laurent.perrinet@univ-amu.fr

Gabriel Peyré
CNRS and Ceremade
Univ. Paris-Dauphine
75775 Paris Cedex 16, FRANCE
peyre@ceremade.dauphine.fr

Abstract

Perception is often described as a predictive process based on an optimal inference with respect to a generative model. We study here the principled construction of a generative model specifically crafted to probe motion perception. In that context, we first provide an axiomatic, biologically-driven derivation of the model. This model synthesizes random dynamic textures which are defined by stationary Gaussian distributions obtained by the random aggregation of warped patterns. Importantly, we show that this model can equivalently be described as a stochastic partial differential equation. Using this characterization of motion in images, it allows us to recast motion-energy models into a principled Bayesian inference framework. Finally, we apply these textures in order to psychophysically probe speed perception in humans. In this framework, while the likelihood is derived from the generative model, the prior is estimated from the observed results and accounts for the perceptual bias in a principled fashion.

1 Motivation

A normative explanation for the function of perception is to infer relevant hidden parameters from the sensory input with respect to a generative model [7]. Equipped with some prior knowledge about this representation, this corresponds to the *Bayesian brain* hypothesis, as has been perfectly illustrated by the particular case of motion perception [19]. However, the Gaussian hypothesis related to the parameterization of knowledge in these models —for instance in the formalization of the prior and of the likelihood functions— does not always fit with psychophysical results [17]. As such, a major challenge is to refine the definition of generative models so that they conform to the widest variety of results.

From this observation, the estimation problem inherent to perception is linked to the definition of an adequate generative model. In particular, the simplest generative model to describe visual motion is the luminance conservation equation. It states that luminance $I(x, t)$ for $(x, t) \in \mathbb{R}^2 \times \mathbb{R}$ is approximately conserved along trajectories defined as integral lines of a vector field $v(x, t) \in \mathbb{R}^2 \times \mathbb{R}$. The corresponding generative model defines random fields as solutions to the stochastic partial differential equation (SPDE),

$$\langle v, \nabla I \rangle + \frac{\partial I}{\partial t} = W, \quad (1)$$

where $\langle \cdot, \cdot \rangle$ denotes the Euclidean scalar product in \mathbb{R}^2 , ∇I is the spatial gradient of I . To match the statistics of natural scenes or some category of textures, the driving term W is usually defined as a colored noise corresponding to some average spatio-temporal coupling, and is parameterized by a covariance matrix Σ , while the field is usually a constant vector $v(x, t) = v_0$ accounting for a full-field translation with constant speed.

Ultimately, the application of this generative model is essential for probing the visual system, for instance to understand how observers might detect motion in a scene. Indeed, as shown by [9, 19], the negative log-likelihood corresponding to the luminance conservation model (1) and determined by a hypothesized speed v_0 is proportional to the value of the motion-energy model [1] $\|\langle v_0, \nabla(K \star I) \rangle + \frac{\partial(K \star I)}{\partial t} \|^2$, where K is the whitening filter corresponding to the inverse of Σ , and \star is the convolution operator. Using some prior knowledge on the distribution of motions, for instance a preference for slow speeds, this indeed leads to a Bayesian formalization of this inference problem [18]. This has been successful in accounting for a large class of psychophysical observations [19]. As a consequence, such probabilistic frameworks allow one to connect different models from computer vision to neuroscience with a unified, principled approach.

However the model defined in (1) is obviously quite simplistic with respect to the complexity of natural scenes. It is therefore useful here to relate this problem to solutions proposed by texture synthesis methods in the computer vision community. Indeed, the literature on the subject of static textures synthesis is abundant (see [16] and the references therein for applications in computer graphics). Of particular interest for us is the work of Galerne et al. [6], which proposes a stationary Gaussian model restricted to static textures. Realistic dynamic texture models are however less studied, and the most prominent method is the non-parametric Gaussian auto-regressive (AR) framework of [3], which has been refined in [20].

Contributions. Here, we seek to engender a better understanding of motion perception by improving generative models for dynamic texture synthesis. From that perspective, we motivate the generation of optimal stimulation within a stationary Gaussian dynamic texture model. We base our model on a previously defined heuristic [10, 11] coined “Motion Clouds”. Our first contri-

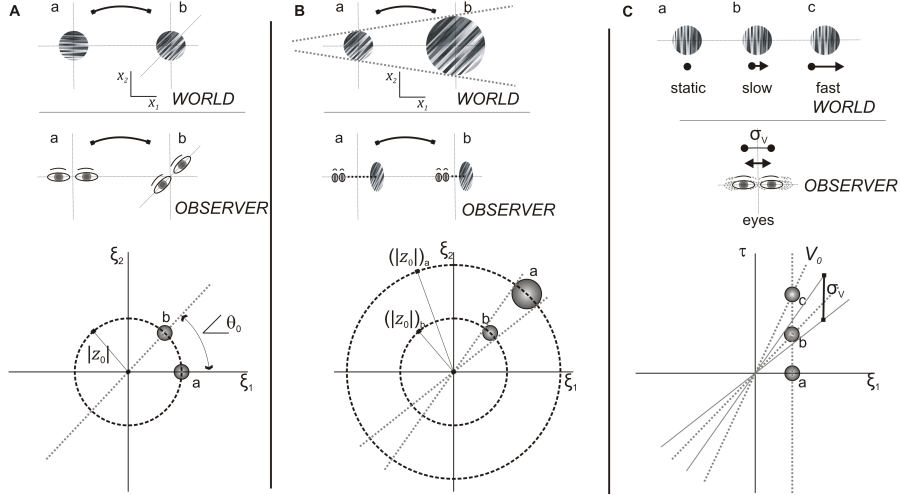


Figure 1: Parameterization of the class of Motion Clouds stimuli. The illustration relates the parametric changes in MC with real world (top row) and observer (second row) movements. (A) Orientation changes resulting in scene rotation are parameterized through θ as shown in the bottom row where a horizontal a and obliquely oriented b MC are compared. (B) Zoom movements, either from scene looming or observer movements in depth, are characterised by scale changes reflected by a scale or frequency term z shown for a larger or closer object b compared to more distant a . (C) Translational movements in the scene characterised by V using the same formulation for static (a) slow (b) and fast moving MC, with the variability in these speeds quantified by σ_V . (ξ and τ) in the third row are the spatial and temporal frequency scale parameters. The development of this formulation is detailed in the text.

bution is an axiomatic derivation of this model, seen as a shot noise aggregation of dynamically warped “textons”. This formulation is important to provide a clear understanding of the effects of the model’s parameters manipulated during psychophysical experiments. Within our generative model, they correspond to average translation speed and orientation of the “textons” and standard deviations of random fluctuations around this average. Our second contribution is to demonstrate an explicit equivalence between this model and a class of linear stochastic partial differential equations (sPDE). This shows that our model is a generalization of the well-known luminance conservation equation. This sPDE formulation has two chief advantages: it allows for a real-time synthesis using an AR recurrence and it allows one to recast the log-likelihood of the model as a generalization of the classical motion energy model, which in turn is crucial to allow for a Bayesian modeling of perceptual biases. Our last contribution is an illustrative application of this model to the psychophysical study of motion perception in humans. This application shows how the model allows us to define a likelihood, which enables a simple fitting procedure to determine the prior driving the perceptual bias.

Notations. In the following, we will denote $(x, t) \in \mathbb{R}^2 \times \mathbb{R}$ the space/time variable, and $(\xi, \tau) \in \mathbb{R}^2 \times \mathbb{R}$ the corresponding frequency variables. If $f(x, t)$ is a function defined on \mathbb{R}^3 , then $\hat{f}(\xi, \tau)$ denotes its Fourier transform. For $\xi \in \mathbb{R}^2$, we denote $\xi = \|\xi\|(\cos(\angle\xi), \sin(\angle\xi)) \in \mathbb{R}^2$ its polar coordinates. For a function g in \mathbb{R}^2 , we denote $\bar{g}(x) = g(-x)$. In the following, we denote with a capital letter such as A a random variable, a we denote a a realization of A , we let $\mathbb{P}_A(a)$ be the corresponding distribution of A .

2 Axiomatic Construction of a Dynamic Texture Stimulation Model

Solving a model-based estimation problem and finding optimal dynamic textures for stimulating an instance of such a model can be seen as equivalent mathematical problems. In the luminance conservation model (1), the generative model is parameterized by a spatio-temporal coupling function, which is encoded in the covariance Σ of the driving noise and the motion flow v_0 . This coupling (covariance) is essential as it quantifies the extent of the spatial integration area as well as the integration dynamics, an important issue in neuroscience when considering the implementation of integration mechanisms from the local to the global scale. In particular, it is important to understand modular sensitivity in the various lower visual areas with different spatio-temporal selectivities such as Primary Visual Cortex (V1) or ascending the processing hierarchy, Middle Temple area (MT). For instance, by varying the frequency bandwidth of such dynamic textures, distinct mechanisms for perception and action have been identified [11]. However, such textures were based on a heuristic [10], and our goal here is to develop a principled, axiomatic definition.

2.1 From Shot Noise to Motion Clouds

We propose a mathematically-sound derivation of a general parametric model of dynamic textures. This model is defined by aggregation, through summation, of a basic spatial “texton” template $g(x)$. The summation reflects a transparency hypothesis, which has been adopted for instance in [6]. While one could argue that this hypothesis is overly simplistic and does not model occlusions or edges, it leads to a tractable framework of stationary Gaussian textures, which has proved useful to model static micro-textures [6] and dynamic natural phenomena [20]. The simplicity of this framework allows for a fine tuning of frequency-based (Fourier) parameterization, which is desirable for the interpretation of psychophysical experiments.

We define a random field as

$$I_\lambda(x, t) \stackrel{\text{def.}}{=} \frac{1}{\sqrt{\lambda}} \sum_{p \in \mathbb{N}} g(\varphi_{A_p}(x - X_p - V_p t)) \quad (2)$$

where $\varphi_a : \mathbb{R}^2 \rightarrow \mathbb{R}^2$ is a planar warping parameterized by a finite dimensional vector a . Intuitively, this model corresponds to a dense mixing of stereotyped, static textons as in [6]. The originality is two-fold. First, the components of this mixing are derived from the texton by visual transformations φ_{A_p} which may correspond to arbitrary transformations such as zooms or rotations, illustrated in Figure 1. Second, we explicitly model the motion (position X_p and speed V_p) of each individual texton. The parameters $(X_p, V_p, A_p)_{p \in \mathbb{N}}$ are independent random vectors. They account for the

variability in the position of objects or observers and their speed, thus mimicking natural motions in an ambient scene. The set of translations $(X_p)_{p \in \mathbb{N}}$ is a 2-D Poisson point process of intensity $\lambda > 0$. The following section instantiates this idea and proposes canonical choices for these variabilities. The warping parameters $(A_p)_p$ are distributed according to a distribution \mathbb{P}_A . The speed parameters $(V_p)_p$ are distributed according to a distribution \mathbb{P}_V on \mathbb{R}^2 . The following result shows that the model (2) converges to a stationary Gaussian field and gives the parameterization of the covariance. Its proof follows from a specialization of [5, Theorem 3.1] to our setting.

Proposition 1. *I_λ is stationary with bounded second order moments. Its covariance is $\Sigma(x, t, x', t') = \gamma(x - x', t - t')$ where γ satisfies*

$$\forall (x, t) \in \mathbb{R}^3, \quad \gamma(x, t) = \int \int_{\mathbb{R}^2} c_g(\varphi_a(x - \nu t)) \mathbb{P}_V(\nu) \mathbb{P}_A(a) d\nu da \quad (3)$$

where $c_g = g \star \bar{g}$ is the auto-correlation of g . When $\lambda \rightarrow +\infty$, it converges (in the sense of finite dimensional distributions) toward a stationary Gaussian field I of zero mean and covariance Σ .

2.2 Definition of “Motion Clouds”

We detail this model here with warpings as rotations and scalings (see Figure 1). These account for the characteristic orientations and sizes (or spatial scales) in a scene with respect to the observer

$$\forall a = (\theta, z) \in [-\pi, \pi) \times \mathbb{R}_+^*, \quad \varphi_a(x) \stackrel{\text{def}}{=} z R_{-\theta}(x),$$

where R_θ is the planar rotation of angle θ . We now give some physical and biological motivation underlying our particular choice for the distributions of the parameters. We assume that the distributions \mathbb{P}_Z and \mathbb{P}_Θ of spatial scales z and orientations θ , respectively (see Figure 1), are independent and have densities, thus considering

$$\forall a = (\theta, z) \in [-\pi, \pi) \times \mathbb{R}_+^*, \quad \mathbb{P}_A(a) = \mathbb{P}_Z(z) \mathbb{P}_\Theta(\theta).$$

The speed vector ν is assumed to be randomly fluctuating around a central speed v_0 , so that

$$\forall \nu \in \mathbb{R}^2, \quad \mathbb{P}_V(\nu) = \mathbb{P}_{\|V - v_0\|}(\|\nu - v_0\|). \quad (4)$$

In order to obtain “optimal” responses to the stimulation (as advocated by [21]), it makes sense to define the texton g to be equal to an oriented Gabor acting as an atom, based on the structure of a standard receptive field of V1. Each would have a scale σ and a central frequency ξ_0 . Since the orientation and scale of the texton is handled by the (θ, z) parameters, we can impose without loss of generality the normalization $\xi_0 = (1, 0)$. In the special case where $\sigma \rightarrow 0$, g is a grating of frequency ξ_0 , and the image I is a dense mixture of drifting gratings, whose power-spectrum has a closed form expression detailed in Proposition 2. Its proof can be found in Section D.1. We call this Gaussian field a Motion Cloud (MC), and it is parameterized by the envelopes $(\mathbb{P}_Z, \mathbb{P}_\Theta, \mathbb{P}_V)$ and has central frequency and speed (ξ_0, v_0) . Note that it is possible to consider any arbitrary textons g , which would give rise to more complicated parameterizations for the power spectrum \hat{g} , but we decided here to stick to the simple case of gratings.

Proposition 2. *When $g(x) = e^{i\langle x, \xi_0 \rangle}$, the image I defined in Proposition 1 is a stationary Gaussian field of covariance having the power-spectrum*

$$\forall (\xi, \tau) \in \mathbb{R}^2 \times \mathbb{R}, \quad \hat{\gamma}(\xi, \tau) = \frac{\mathbb{P}_Z(\|\xi\|)}{\|\xi\|^2} \mathbb{P}_\Theta(\angle \xi) \mathcal{L}(\mathbb{P}_{\|V - v_0\|}) \left(-\frac{\tau + \langle v_0, \xi \rangle}{\|\xi\|} \right), \quad (5)$$

where the linear transform \mathcal{L} is such that $\forall u \in \mathbb{R}, \mathcal{L}(f)(u) = \int_{-\pi}^{\pi} f(-u / \cos(\varphi)) d\varphi$.

Remark 1. Note that the envelope of $\hat{\gamma}$ is shaped along a cone in the spatial and temporal domains. This is an important and novel contribution when compared to a Gaussian formulation like a classical Gabor. In particular, the bandwidth is then constant around the speed plane or the orientation line with respect to spatial frequency. Basing the generation of the textures on all possible translations, rotations and zooms, we thus provide a principled approach to show that bandwidth should be proportional to spatial frequency to provide a better model of moving textures.

2.3 Biologically-inspired Parameter Distributions

We now give meaningful specialization for the probability distributions $(\mathbb{P}_Z, \mathbb{P}_\Theta, \mathbb{P}_{\|V-v_0\|})$, which are inspired by some known scaling properties of the visual transformations relevant to dynamic scene perception.

First, small, centered, linear movements of the observer along the axis of view (orthogonal to the plane of the scene) generate centered planar zooms of the image. From the linear modeling of the observer's displacement and the subsequent multiplicative nature of zoom, scaling should follow a Weber-Fechner law stating that subjective sensation when quantified is proportional to the logarithm of stimulus intensity. Thus, we choose the scaling z drawn from a log-normal distribution \mathbb{P}_Z , defined in (6). The bandwidth σ_Z quantifies the variance in the amplitude of zooms of individual textons relative to the set characteristic scale z_0 . Similarly, the texture is perturbed by variation in the global angle θ of the scene: for instance, the head of the observer may roll slightly around its normal position. The von-Mises distribution – as a good approximation of the warped Gaussian distribution around the unit circle – is an adapted choice for the distribution of θ with mean θ_0 and bandwidth σ_Θ , see (6). We may similarly consider that the position of the observer is variable in time. On first order, movements perpendicular to the axis of view dominate, generating random perturbations to the global translation v_0 of the image at speed $v - v_0 \in \mathbb{R}^2$. These perturbations are for instance described by a Gaussian random walk: take for instance tremors, which are constantly jittering, small (≤ 1 deg) movements of the eye. This justifies the choice of a radial distribution (4) for \mathbb{P}_V . This radial distribution $\mathbb{P}_{\|V-v_0\|}$ is thus selected as a bell-shaped function of width σ_V , and we choose here a Gaussian function for simplicity, see (6). Note that, as detailed in Section B.3 a slightly different bell-function (with a more complicated expression) should be used to obtain an exact equivalence with the sPDE discretization mentioned in Section 2.4.

The distributions of the parameters are thus chosen as

$$\mathbb{P}_Z(z) \propto \frac{z_0}{z} e^{-\frac{\ln(\frac{z}{z_0})^2}{2 \ln(1+\sigma_Z^2)}}, \quad \mathbb{P}_\Theta(\theta) \propto e^{\frac{\cos(2(\theta-\theta_0))}{4\sigma_\Theta^2}} \quad \text{and} \quad \mathbb{P}_{\|V-v_0\|}(r) \propto e^{-\frac{r^2}{2\sigma_V^2}}. \quad (6)$$

Remark 2. Note that in practice we have parametrized \mathbb{P}_Z by its mode $m_Z = \arg\max_z \mathbb{P}_Z(z)$ and standard deviation $d_Z = \sqrt{\int z^2 \mathbb{P}_Z(z) dz}$, see Section B.4 and [4].

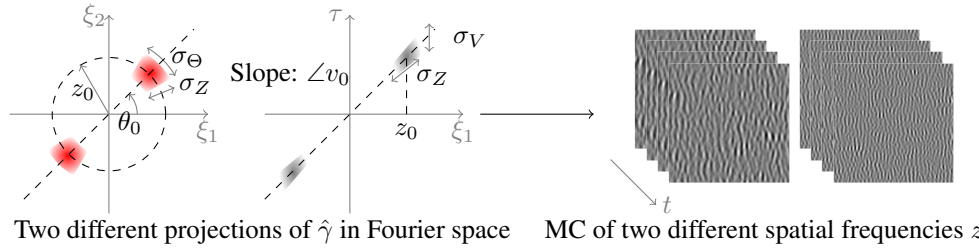


Figure 2: Graphical representation of the covariance γ (left) —note the cone-like shape of the envelopes— and an example of synthesized dynamics for narrow-band and broad-band Motion Clouds (right).

Plugging these expressions (6) into the definition (5) of the power spectrum of the motion cloud, one obtains a parameterization which is very similar to the one originally introduced in [11]. The following table gives the speed v_0 and frequency (θ_0, z_0) central parameters in terms of amplitude and orientation, each one being coupled with the relevant dispersion parameters. Figure 1 and 2 shows a graphical display of the influence of these parameters.

	Speed	Freq. orient.	Freq. amplitude
(mean, dispersion)	(v_0, σ_V)	$(\theta_0, \sigma_\Theta)$	(z_0, σ_Z) or (m_Z, d_Z)

Remark 3. Note that the final envelope of $\hat{\gamma}$ is in agreement with the formulation that is used in [10]. However, that previous derivation was based on a heuristic which intuitively emerged from a long interaction between modelers and psychophysicists. Herein, we justified these different points from first principles.

2.4 sPDE Formulation and Numerical Synthesis Algorithm

The MC model can equally be described as a stationary solution of a stochastic partial differential equation (sPDE). This sPDE formulation is important since we aim to deal with dynamic stimulation, which should be described by a causal equation which is local in time. This is crucial for numerical simulations, since, this allows us to perform real-time synthesis of stimuli using an auto-regressive time discretization. This is a significant departure from previous Fourier-based implementation of dynamic stimulation [10, 11]. This is also important to simplify the application of MC inside a bayesian model of psychophysical experiments (see Section 3) The derivation of an equivalent sPDE model exploits a spectral formulation of MCs as Gaussian Random fields. The full proof along with the synthesis algorithm can be found in Section 2.4.

3 Psychophysical Study: Speed Discrimination

To exploit the useful features of our MC model and provide a generalizable proof of concept based on motion perception, we consider here the problem of judging the relative speed of moving dynamical textures and the impact of both average spatial frequency and average duration of temporal correlations.

3.1 Methods

The task was to discriminate the speed $v \in \mathbb{R}$ of MC stimuli moving with a horizontal central speed $v_0 = (v, 0)$. We assign as independent experimental variable the most represented spatial frequency m_Z , that we denote in the following z for easier reading. The other parameters are set to the following values

$$\sigma_V = \frac{1}{t^* z_0}, \quad \theta_0 = \frac{\pi}{2}, \quad \sigma_\Theta = \frac{\pi}{12}, \quad d_Z = 1.0 \text{ c}^\circ.$$

Note that σ_V is thus dependent of the value of z_0 (that is computed from m_Z and d_Z , see Remark 2 and Section B.4) to ensure that $t^* = \frac{1}{\sigma_V z_0}$ stays constant. This parameter t^* controls the temporal frequency bandwidth, as illustrated on the middle of Figure 2. We used a two alternative forced choice (2AFC) paradigm. In each trial a grey fixation screen with a small dark fixation spot was followed by two stimulus intervals of 250 ms each, separated by a grey 250 ms inter-stimulus interval. The first stimulus had parameters (v_1, z_1) and the second had parameters (v_2, z_2) . At the end of the trial, a grey screen appeared asking the participant to report which one of the two intervals was perceived as moving faster by pressing one of two buttons, that is whether $v_1 > v_2$ or $v_2 > v_1$.

Given reference values (v^*, z^*) , for each trial, (v_1, z_1) and (v_2, z_2) are selected so that

$$\begin{cases} v_i = v^*, z_i \in z^* + \Delta_Z \\ v_j \in v^* + \Delta_V, z_j = z^* \end{cases} \quad \text{where} \quad \begin{cases} \Delta_V = \{-2, -1, 0, 1, 2\}, \\ \Delta_Z = \{-0.48, -0.21, 0, 0.32, 0.85\}, \end{cases}$$

where $(i, j) = (1, 2)$ or $(i, j) = (2, 1)$ (i.e. the ordering is randomized across trials), and where z values are expressed in cycles per degree (c°) and v values in $^\circ/\text{s}$. Ten repetitions of each of the 25 possible combinations of these parameters are made per block of 250 trials and at least four such blocks were collected per condition tested. The outcome of these experiments are summarized by psychometric curves $\hat{\varphi}_{v^*, z^*}$, where for all $(v - v^*, z - z^*) \in \Delta_V \times \Delta_Z$, the value $\hat{\varphi}_{v^*, z^*}(v, z)$ is the empirical probability (each averaged over the typically 40 trials) that a stimulus generated with parameters (v^*, z) is moving faster than a stimulus with parameters (v, z^*) .

To assess the validity of our model, we tested four different scenarios by considering all possible choices among

$$z^* = 1.28 \text{ c}^\circ, \quad v^* \in \{5^\circ/\text{s}, 10^\circ/\text{s}\}, \quad t^* \in \{0.1\text{s}, 0.2\text{s}\},$$

which corresponds to combinations of low/high speeds and a pair of temporal frequency parameters. Stimuli were generated on a Mac running OS 10.6.8 and displayed on a 20" Viewsonic p227f monitor with resolution 1024×768 at 100 Hz. Routines were written using Matlab 7.10.0 and Psychtoolbox 3.0.9 controlled the stimulus display. Observers sat 57 cm from the screen in a dark room. Three observers with normal or corrected to normal vision took part in these experiments. They gave their informed consent and the experiments received ethical approval from the Aix-Marseille Ethics Committee in accordance with the declaration of Helsinki.

3.2 Bayesian modeling

To make full use of our MC paradigm in analyzing the obtained results, we follow the methodology of the Bayesian observer used for instance in [13, 12, 8]. We assume the observer makes its decision using a Maximum A Posteriori (MAP) estimator

$$\hat{v}_z(m) = \underset{v}{\operatorname{argmin}} [-\log(\mathbb{P}_{M|V,Z}(m|v, z)) - \log(\mathbb{P}_{V|Z}(v|z))] \quad (7)$$

computed from some internal representation $m \in \mathbb{R}$ of the observed stimulus. For simplicity, we assume that the observer estimates z from m without bias. To simplify the numerical analysis, we assume that the likelihood is Gaussian, with a variance independent of v . Furthermore, we assume that the prior is Laplacian as this gives a good description of the a priori statistics of speeds in natural images [2]:

$$\mathbb{P}_{M|V,Z}(m|v, z) = \frac{1}{\sqrt{2\pi}\sigma_z} e^{-\frac{|m-v|^2}{2\sigma_z^2}} \quad \text{and} \quad \mathbb{P}_{V|Z}(v|z) \propto e^{a_z v} 1_{[0, v_{\max}]}(v). \quad (8)$$

where $v_{\max} > 0$ is a cutoff speed ensuring that $\mathbb{P}_{V|Z}$ is a well defined density even if $a_z > 0$. Both a_z and σ_z are unknown parameters of the model, and are obtained from the outcome of the experiments by a fitting process we now explain.

3.3 Likelihood and Prior Estimation

Following for instance [13, 12, 8], the theoretical psychophysical curve obtained by a Bayesian decision model is

$$\varphi_{v^*, z^*}(v, z) \stackrel{\text{def}}{=} \mathbb{E}(\hat{v}_{z^*}(M_{v, z^*}) > \hat{v}_z(M_{v^*, z}))$$

where $M_{v, z} \sim \mathcal{N}(v, \sigma_z^2)$ is a Gaussian variable having the distribution $\mathbb{P}_{M|V,Z}(\cdot|v, z)$.

The following proposition shows that in our special case of Gaussian prior and Laplacian likelihood, it can be computed in closed form. Its proof follows closely the derivation of [12, Appendix A], and can be found in Section D.2.

Proposition 3. *In the special case of the estimator (7) with a parameterization (8), one has*

$$\varphi_{v^*, z^*}(v, z) = \psi \left(\frac{v - v^* - a_{z^*} \sigma_{z^*}^2 + a_z \sigma_z^2}{\sqrt{\sigma_{z^*}^2 + \sigma_z^2}} \right) \quad (9)$$

where $\psi(t) = \frac{1}{\sqrt{2\pi}} \int_{-\infty}^t e^{-s^2/2} ds$ is a sigmoid function.

One can fit the experimental psychometric function to compute the perceptual bias term $\mu_{z, z^*} \in \mathbb{R}$ and an uncertainty λ_{z, z^*} such that

$$\hat{\varphi}_{v^*, z^*}(v, z) \approx \psi \left(\frac{v - v^* - \mu_{z, z^*}}{\lambda_{z, z^*}} \right). \quad (10)$$

Remark 4. Note that in practice we perform a fit in a log-speed domain *ie* we consider $\varphi_{\tilde{v}^*, z^*}(\tilde{v}, z)$ where $\tilde{v} = \ln(1 + v/v_0)$ with $v_0 = 0.3^\circ/\text{s}$ following [13].

By comparing the theoretical and experimental psychophysical curves (9) and (10), one thus obtains the following expressions

$$\sigma_z^2 = \lambda_{z, z^*}^2 - \frac{1}{2} \lambda_{z^*, z^*}^2 \quad \text{and} \quad a_z = a_{z^*} \frac{\sigma_{z^*}^2}{\sigma_z^2} - \frac{\mu_{z, z^*}}{\sigma_z^2}.$$

The only remaining unknown is a_{z^*} , that can be set as any negative number based on previous work on low speed priors or, alternatively estimated in future by performing a wiser fitting method.

3.4 Psychophysic Results

The main results are summarized in Figure 3 showing the parameters μ_{z, z^*} in Figure 3(a) and the parameters σ_z in Figure 3(b). Spatial frequency has a positive effect on perceived speed; speed is systematically perceived as faster as spatial frequency is increased, moreover this shift cannot simply

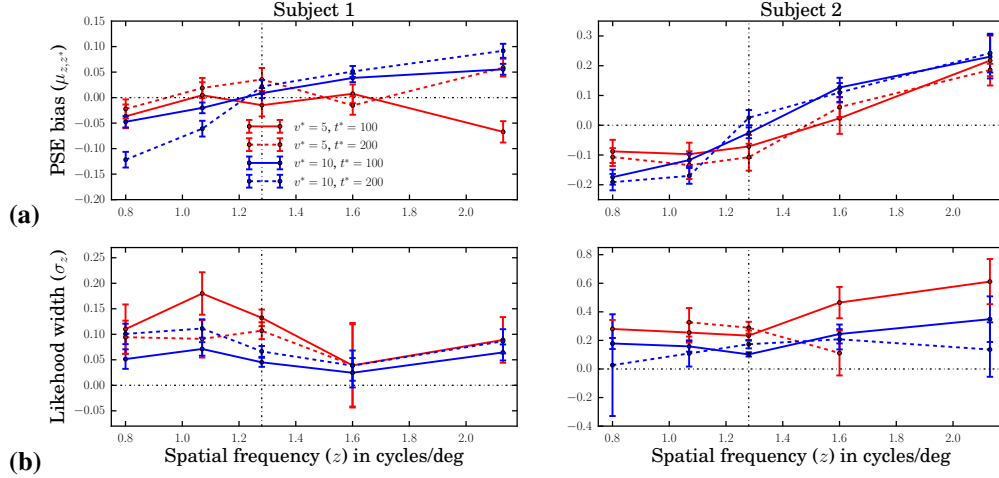


Figure 3: 2AFC speed discrimination results. (a) Task generates psychometric functions which show shifts in the point of subjective equality for the range of test z . Stimuli of lower frequency with respect to the reference (intersection of dotted horizontal and vertical lines gives the reference stimulus) are perceived as going slower, those with greater mean frequency are perceived as going relatively faster. This effect is observed under all conditions but is stronger at the highest speed and for subject 1. (b) The estimated σ_z appear noisy but roughly constant as a function of z for each subject. Widths are generally higher for $v = 5$ (red) than $v = 10$ (blue) traces. The parameter t^* does not show a significant effect across the conditions tested.

be explained to be the result of an increase in the likelihood width (Figure 3(b)) at the tested spatial frequency, as previously observed for contrast changes [13, 12]. Therefore the positive effect could be explained by a negative effect in prior slopes a_z as the spatial frequency increases. However, we do not have any explanation for the observed constant likelihood width as it is not consistent with the speed width of the stimuli $\sigma_V = \frac{1}{t^* z_0}$ which is decreasing with spatial frequency.

3.5 Discussion

We exploited the principled and ecologically motivated parameterization of MC to ask about the effect of scene scaling on speed judgements. In the experimental task, MC stimuli, in which the spatial scale content was systematically varied (via frequency manipulations) around a central frequency of 1.28 c/° were found to be perceived as slightly faster at higher frequencies slightly slower at lower frequencies. The effects were most prominent at the faster speed tested, of 10 °/s relative to those at 5 °/s. The fitted psychometric functions were compared to those predicted by a Bayesian model in which the likelihood or the observer’s sensory representation was characterised by a simple Gaussian. Indeed, for this small data set intended as a proof of concept, the model was able to explain these systematic biases for spatial frequency as shifts in our *a priori* on speed during the perceptual judgements as the likelihood width are constant across tested frequencies but lower at the higher of the tested speeds. Thus having a larger measured bias given the case of the smaller likelihood width (faster speed) is consistent with a key role for the prior in the observed perceptual bias.

A larger data set, including more standard spatial frequencies and the use of more observers, is needed to disambiguate the models predicted prior function.

4 Conclusions

We have proposed and detailed a generative model for the estimation of the motion of images based on a formalization of small perturbations from the observer’s point of view during parameterized rotations, zooms and translations. We connected these transformations to descriptions of ecologically motivated movements of both observers and the dynamic world. The fast synthesis of naturalistic textures optimized to probe motion perception was then demonstrated, through fast GPU implementations applying auto-regression techniques with much potential for future experimenta-

tion. This extends previous work from [10] by providing an axiomatic formulation. Finally, we used the stimuli in a psychophysical task and showed that these textures allow one to further understand the processes underlying speed estimation. By linking them directly to the standard Bayesian formalism, we show that the sensory representations of the stimulus (the likelihoods) in such models can be described directly from the generative MC model. In our case we showed this through the influence of spatial frequency on speed estimation. We have thus provided just one example of how the optimised motion stimulus and accompanying theoretical work might serve to improve our understanding of inference behind perception.

Acknowledgements

We thank Guillaume Masson for useful discussions during the development of the experiments. We also thank Manon Bouyé and Élise Amfreville for proofreading. LUP was supported by EC FP7-269921, “BrainScales”. The work of JV and GP was supported by the European Research Council (ERC project SIGMA-Vision). AIM and LUP were supported by SPEED ANR-13-SHS2-0006.

A Graphical Display of MC

We recall that MC are stationary Gaussian random field with a parameterized power spectrum having the form

$$\forall (\xi, \tau) \in \mathbb{R}^3, \hat{\gamma}(\xi, \tau) = \frac{\mathbb{P}_Z(\|\xi\|)}{\|\xi\|^2} \mathbb{P}_\Theta(\angle \xi) \mathcal{L}(\mathbb{P}_{\|V - v_0\|}) \left(\|v_0\| \cos(\angle v_0 - \angle \xi) - \frac{\tau}{\|\xi\|} \right). \quad (11)$$

Similarly as was previously proposed in [10]. We show in Figure 4 two examples of such stimuli for different spatial frequency bandwidths. In particular, by tuning this bandwidth we could dissociate their respective role in action and perception [10, 11]. Extending the study of visual perception to other dimensions, such as orientation or speed bandwidths, should provide essential data to titrate their respective role in motion integration.

B sPDE Formulation and Numerics

The formulation of the MC gives an explicit parameterization (11) of the covariance over the Fourier domain. We show here that it can be equivalently discretized by the solutions of a local PDE driven by a Gaussian noise. This formulation is important since we aim to deal with dynamic stimulation, which should be described by a causal equation which is local in time. This is indeed crucial to offer a fast simulation algorithm (see Section B.5) and to offer a coherent Bayesian inference framework, as shown in Section C.

B.1 Dynamic Textures as Solutions of sPDE

A MC I with speed v_0 can be obtained from a MC I_0 with zero speed by the constant speed time warping

$$I(x, t) \stackrel{\text{def.}}{=} I_0(x - v_0 t, t). \quad (12)$$

We now restrict our attention to I_0 .

We consider Gaussian random fields defined by a stochastic partial differential equation (sPDE) of the form

$$\mathcal{D}(I_0) = \frac{\partial W}{\partial t}(x) \quad \text{where} \quad \mathcal{D}(I_0) \stackrel{\text{def.}}{=} \frac{\partial^2 I_0}{\partial t^2}(x) + \alpha \star \frac{\partial I_0}{\partial t}(x) + \beta \star I_0(x) \quad (13)$$

This equation should be satisfied for all (x, t) , and we look for Gaussian fields that are stationary solutions of this equation. In this sPDE, the driving noise $\frac{\partial W}{\partial t}$ is white in time (i.e. corresponding to the temporal derivative of a Brownian motion in time) and has a 2-D covariance Σ_W in space and \star is the spatial convolution operator. The parameters (α, β) are 2-D spatial filters that aim at enforcing an additional correlation in time of the model. Section B.2 explains how to choose $(\alpha, \beta, \Sigma_W)$ so

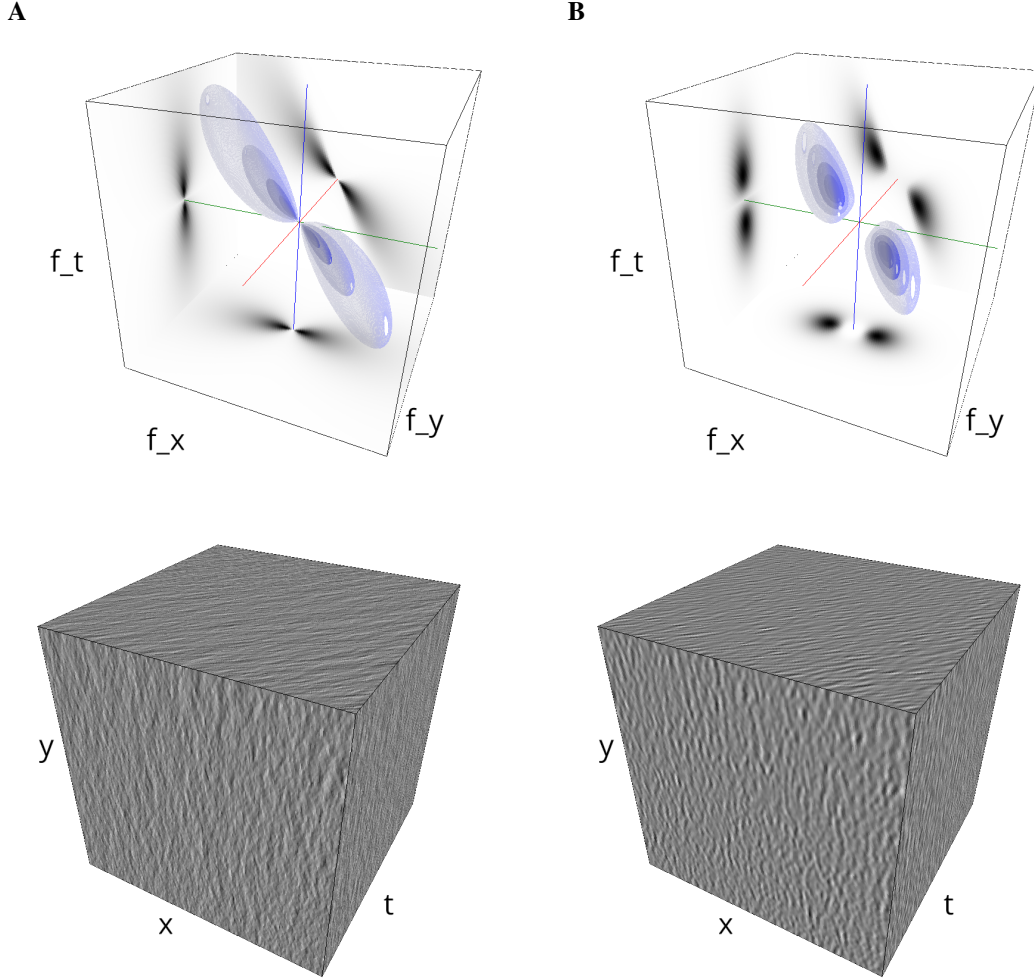


Figure 4: Broadband vs. narrowband stimuli. We show in **(A)** and **(B)** instances of the same Motion Clouds with different frequency bandwidths σ_Z , while all other parameters (such as z_0) are kept constant. The top column displays iso-surfaces of the spectral envelope by displaying enclosing volumes at different energy values with respect to the peak amplitude of the Fourier spectrum. The bottom column shows an isometric view of the faces of the movie cube. The first frame of the movie lies on the x-y plane, the x-t plane lies on the top face and motion direction is seen as diagonal lines on this face (vertical motion is similarly seen in the y-t face). The Motion Cloud with the broadest bandwidth is thought to best represent natural stimuli, since, as those, it contains many frequency components. **(A)** $\sigma_Z = 0.25$, **(B)** $\sigma_Z = 0.0625$.

that the stationary solutions of (13) have the power spectrum given in (11) (in the case that $v_0 = 0$), i.e. are motion clouds.

This sPDE formulation is important since we aim to deal with dynamic stimulation, which should be described by a causal equation which is local in time. This is crucial for numerical simulation (as explained in Section B.5) but also to simplify the application of MC inside a bayesian model of psychophysical experiments (see Section C).

While it is beyond the scope of this paper to study theoretically this equation, one can show existence and uniqueness results of stationary solutions for this class of sPDE under stability conditions on the filters (α, β) (see for instance [14]) that we found numerically to be always satisfied in our simulations. Note also that one can show that in fact the stationary solutions to (13) all share the same law. These solutions can be obtained by solving the sODE (14) forward for time $t > t_0$ with arbitrary boundary conditions at time $t = t_0$, and letting $t_0 \rightarrow -\infty$. This is consistent with the numerical scheme detailed in Section B.5.

B.2 Equivalence Between Spectral and sPDE MC Formulations

The sPDE equation (13) corresponds to a set of independent stochastic ODEs over the spatial Fourier domain, which reads, for each frequency ξ ,

$$\forall t \in \mathbb{R}, \quad \frac{\partial^2 \hat{I}_0(\xi, t)}{\partial t^2} + \hat{\alpha}(\xi) \frac{\partial \hat{I}_0(\xi, t)}{\partial t} + \hat{\beta}(\xi) \hat{I}_0(\xi, t) = \hat{\sigma}_W(\xi) \hat{w}(\xi, t) \quad (14)$$

where $\hat{I}_0(\xi, t)$ denotes the Fourier transform with respect to the space variable x only. Here, $\hat{\sigma}_W(\xi)^2$ is the spatial power spectrum of $\frac{\partial W}{\partial t}$, which means that

$$\Sigma_W(x, y) = c(x - y) \quad \text{where} \quad \hat{c}(\xi) = \hat{\sigma}_W^2(\xi). \quad (15)$$

Here $\hat{w}(\xi, t) \sim \mathcal{N}(0, 1)$ and w is a white noise in space and time. This formulation makes explicit that $(\hat{\alpha}(\xi), \hat{\beta}(\xi))$ should be chosen in order to make the temporal covariance of the resulting process equal (or at least approximate) the temporal covariance appearing in (11) in the motion-less setting (since we deal here with I_0), i.e. when $v_0 = 0$. This covariance should be localized around 0 and non-oscillating. It thus makes sense to constrain $(\hat{\alpha}(\xi), \hat{\beta}(\xi))$ for the corresponding ODE (14) to be critically damped, which corresponds to imposing the following relationship

$$\forall \xi, \quad \hat{\alpha}(\xi) = \frac{2}{\hat{\nu}(\xi)} \quad \text{and} \quad \hat{\beta}(\xi) = \frac{1}{\hat{\nu}^2(\xi)}$$

for some relaxation step size $\hat{\nu}(\xi)$. The model is thus solely parameterized by the noise variance $\hat{\sigma}_W(\xi)$ and the characteristic time $\hat{\nu}(\xi)$.

The following proposition shows that the sPDE model (13) and the motion cloud model (11) are identical for an appropriate choice of function $\mathbb{P}_{\|V-v_0\|}$.

Proposition 4. *When considering*

$$\forall r > 0, \quad \mathbb{P}_{\|V-v_0\|}(r) = \mathcal{L}^{-1}(h)(r/\sigma_V) \quad \text{where} \quad h(u) = (1 + u^2)^{-2} \quad (16)$$

where \mathcal{L} is defined in (11), equation (14) admits a solution I which is a stationary Gaussian field with power spectrum (11) when setting

$$\hat{\sigma}_W^2(\xi) = \frac{1}{\hat{\nu}(\xi)\|\xi\|^2} \mathbb{P}_Z(\|\xi\|) \mathbb{P}_\Theta(\angle \xi), \quad \text{and} \quad \hat{\nu}(\xi) = \frac{1}{\sigma_V \|\xi\|}. \quad (17)$$

Proof. For this proof, we denote I^{MC} the motion cloud defined by (11), and I a stationary solution of the sPDE defined by (13). We aim at showing that under the specification (17), they have the same covariance. This is equivalent to show that $I_0^{\text{MC}}(x, t) = I^{\text{MC}}(x + ct, t)$ has the same covariance as I_0 . One shows that for any fixed ξ , equation (14) admits a unique (in law) stationary solution $\hat{I}_0(\xi, \cdot)$ which is a stationary Gaussian process of zero mean and with a covariance which is $\hat{\sigma}_W^2(\xi) r \star \bar{r}$ where r is the impulse response (i.e. taking formally $a = \delta$) of the ODE $r'' + 2r'/u + r''/u^2 = a$ where we denoted $u = \hat{\nu}(\xi)$. This impulse response is easily shown to be $r(t) = te^{-t/u} \mathbb{1}_{\mathbb{R}^+}(t)$. The covariance of $\hat{I}_0(\xi, \cdot)$ is thus, after some computation, equal to $\hat{\sigma}_W^2(\xi) r \star \bar{r} = \hat{\sigma}_W^2(\xi) h(\cdot/u)$ where $h(t) \propto (1 + |t|)e^{-|t|}$. Taking the Fourier transform of this equality, the power spectrum $\hat{\gamma}_0$ of I_0 thus reads

$$\hat{\gamma}_0(\xi, \tau) = \hat{\sigma}_W^2(\xi) \hat{\nu}(\xi) h(\hat{\nu}(\xi) \tau) \quad \text{where} \quad h(u) = \frac{1}{(1 + u^2)^2}$$

and where it should be noted that this h function is the same as the one introduced in (16). The covariance γ^{MC} of I^{MC} and γ_0^{MC} of I_0^{MC} are related by the relation

$$\hat{\gamma}_0^{\text{MC}}(\xi, \tau) = \hat{\gamma}^{\text{MC}}(\xi, \tau - \langle \xi, v_0 \rangle) = \frac{1}{\|\xi\|^2} \mathbb{P}_Z(\|\xi\|) \mathbb{P}_\Theta(\angle \xi) h\left(-\frac{\tau}{\sigma_V \|\xi\|}\right).$$

where we used the expression (11) for $\hat{\gamma}^{\text{MC}}$ and the value of $\mathcal{L}(\mathbb{P}_{\|V-v_0\|})$ given by (16). Condition (17) guarantees that expression (B.2) and (B.2) coincide, and thus $\hat{\gamma}_0 = \hat{\gamma}_0^{\text{MC}}$. \square

B.3 Expression for $\mathbb{P}_{\|V-v_0\|}$

Equation (16) states that in order to obtain a perfect equivalence between the MC defined by (11) and by (13), the function has $\mathcal{L}^{-1}(h)$ to be well-defined. It means we need to compute the inverse of the transform of the linear operator \mathcal{L}

$$\forall u \in \mathbb{R}, \quad \mathcal{L}(f)(u) = 2 \int_0^{\pi/2} f(-u/\cos(\varphi)) d\varphi.$$

to the function h . The following proposition gives a closed-form expression for this function, and shows in particular that it is a function in $L^1(\mathbb{R})$, i.e. it has a finite integral, which can be normalized to unity to define a density distribution. Figure 5 shows a graphical display.

Proposition 5. *One has*

$$\mathcal{L}^{-1}(h)(u) = \frac{2-u^2}{\pi(1+u^2)^2} - \frac{u^2(u^2+4)(\log(u) - \log(\sqrt{u^2+1}+1))}{\pi(u^2+1)^{5/2}}.$$

In particular, one has

$$\mathcal{L}^{-1}(h)(0) = \frac{2}{\pi} \quad \text{and} \quad \mathcal{L}^{-1}(h)(u) \sim \frac{1}{2\pi u^3} \quad \text{when} \quad u \rightarrow +\infty.$$

Proof. The variable substitution $x = \cos(\varphi)$ allows to rewrite (B.3) as

$$\forall u \in \mathbb{R}, \quad \mathcal{L}(h)(u) = 2 \int_0^1 h\left(-\frac{u}{x}\right) \frac{x}{\sqrt{1-x^2}} \frac{dx}{x}.$$

In such a form, we recognize a Mellin convolution which could be inverted by the use of Mellin convolution table. \square

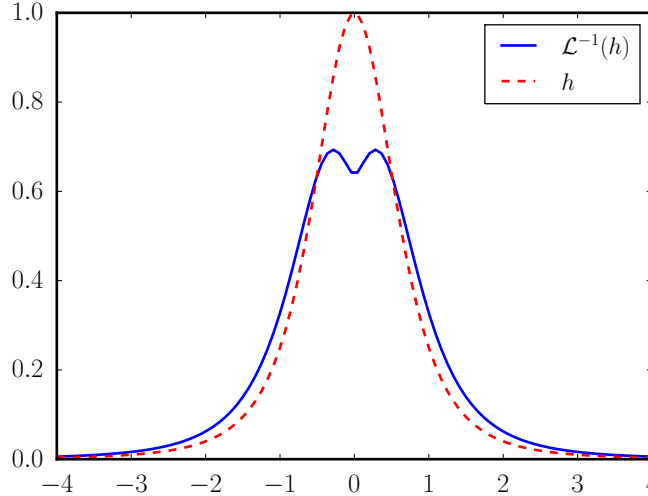


Figure 5: Functions h and $\mathcal{L}^{-1}(h)$.

B.4 Parametrization of \mathbb{P}_Z

Parametrization by mode and standard deviation The log-normal distribution could be written

$$\mathbb{P}_Z(z) \propto \frac{z_0}{z} e^{-\frac{\ln\left(\frac{z}{z_0}\right)^2}{2 \ln\left(1+\sigma_Z^2\right)}}.$$

The parameters (z_0, σ_Z) are convenient to write the distribution but they do not reflect remarkable values of a log-normal random variable. Instead, we prefer to fix directly the mode $m_Z =$

$\operatorname{argmax}_z \mathbb{P}_Z(z)$ and standard deviation $d_Z = \sqrt{\int_{\mathbb{R}_+} z^2 \mathbb{P}_Z(z) dz}$. These couples of variable are linked by the following equations,

$$m_Z = \frac{z_0}{1 + \sigma_Z^2} \quad \text{and} \quad d_Z = z_0 \sigma_Z^2 (1 + \sigma_Z^2).$$

Such formula could be inverted by finding the unique positive root of

$$P(x) = x^2(1 + x^2)^2 - \frac{d_Z}{m_Z}$$

because $P(\sigma_Z) = 0$ and finally set $z_0 = m_Z(1 + \sigma_Z^2)$.

Parametrization by mode and octave bandwidth Another choice would be to parametrize \mathbb{P}_Z by its mode m_Z and octave bandwidth B_Z which is defined by

$$B_Z = \frac{\ln\left(\frac{z_+}{z_-}\right)}{\ln(2)}$$

where (z_-, z_+) are the half-power cutoff frequencies *ie* verifies $\mathbb{P}_Z(z_-) = \mathbb{P}_Z(z_+) = \frac{\mathbb{P}_Z(m_Z)}{2}$. This last condition comes down to study the roots of the following polynomial

$$Q(X) = X^2 + 2 \ln(1 + \sigma_Z^2)X - 2 \ln(2) \ln(1 + \sigma_Z^2) + \frac{1}{2} \ln(1 + \sigma_Z^2)^2$$

where $X = \ln\left(\frac{z}{z_0}\right)$. It follows that

$$B_Z = \sqrt{\frac{8 \ln(1 + \sigma_Z^2)}{\ln(2)}}.$$

Conversely,

$$\sigma_Z = \sqrt{\exp\left(\frac{\ln(2)}{8} B_Z^2\right) - 1}.$$

B.5 AR(2) Discretization of the sPDE

Most previous works (such as [6] for static and [10, 11] for dynamic textures) have used global Fourier-based approach that makes use of the explicit power spectrum expression 11. The main drawbacks of such an approach are: (i) it introduces an artificial periodicity in time and thus can only be used to synthesize a finite number of frames; (ii) the discrete computational grid may introduce artifacts, in particular when one of the bandwidths is of the order of the discretization step; (iii) these frames must be synthesized at once, before the stimulation, which prevents real-time synthesis.

To address these issues, we follow the previous works of [3, 20] and make use of an auto-regressive (AR) discretization of the sPDE (13). In contrast with these previous works, we use a second order AR(2) regression (in place of a first order AR(1) model). Using higher order recursions is crucial to be consistent with the continuous formulation (13). Indeed, numerical simulations show that AR(1) iterations lead to unacceptable temporal artifacts: in particular, the time correlation of AR(1) random fields typically decays too fast in time.

The discretization computes a (possibly infinite) discrete set of 2-D frames $(I_0^{(\ell)})_{\ell \geq \ell_0}$ separated by a time step Δ , and we approach at time $t = \ell \Delta$ the derivatives as

$$\frac{\partial I_0(\cdot, t)}{\partial t} \approx \Delta^{-1} (I_0^{(\ell)} - I_0^{(\ell-1)}) \quad \text{and} \quad \frac{\partial^2 I_0(\cdot, t)}{\partial t^2} \approx \Delta^{-2} (I_0^{(\ell+1)} + I_0^{(\ell-1)} - 2I_0^{(\ell)}),$$

which leads to the following explicit recursion

$$\forall \ell \geq \ell_0, \quad I_0^{(\ell+1)} = (2\delta - \Delta\alpha - \Delta^2\beta) \star I_0^{(\ell)} + (-\delta + \Delta\alpha) \star I_0^{(\ell-1)} + \Delta^2 W^{(\ell)}, \quad (18)$$

where δ is the 2-D Dirac distribution and where $(W^{(\ell)})_\ell$ are i.i.d. 2-D Gaussian field with distribution $\mathcal{N}(0, \Sigma_W)$, and $(I_0^{(\ell_0-1)}, I_0^{(\ell_0-1)})$ can be arbitrary initialized.

One can show that when $\ell_0 \rightarrow -\infty$ (to allow for a long enough “warmup” phase to reach approximate time-stationarity) and $\Delta \rightarrow 0$, then I_0^Δ defined by interpolating $I_0^\Delta(\cdot, \Delta\ell) = I^{(\ell)}$ converges (in the sense of finite dimensional distributions) toward a solution I_0 of the sPDE (13). We refer to [15] for a similar result in the 1-D case (stochastic ODE). We implemented the recursion (18) by computing the 2-D convolutions with FFT’s on a GPU, which allows us to generate high resolution videos in real time, without the need to explicitly store the synthesized video.

C Experimental Likelihood vs. the MC Model

In our paper, we propose to directly fit the likelihood $\mathbb{P}_{M|V,Z}(m|v, z)$ from the experimental psychophysical curve. While this makes sense from a data-analysis point of view, this required strong modeling hypothesis, in particular, that the likelihood is Gaussian with a variance σ_z^2 independent of the parameter v to be estimated by the observer.

In this section, we direct a likelihood model directly from the stimuli, by making another (of course questionable) hypothesis, that the observer uses a standard motion estimation process, based on the motion energy concept [1], that we adapt here to the MC distribution. In this setting, this corresponds to using a MLE estimator, and making use of the sPDE formulation of MC.

C.1 MLE Speed Estimator

We first show how to compute this MLE estimator. To be able to achieve this, the following proposition derive the sPDE satisfied by a motion cloud with a non-zero speed.

Proposition 6. *A MC I with speed v_0 can be defined as a stationary solution of the sPDE*

$$\mathcal{D}(I) + \langle \mathcal{G}(I), v_0 \rangle + \langle \mathcal{H}(I)v_0, v_0 \rangle = \frac{\partial W}{\partial t} \quad (19)$$

where \mathcal{D} is defined in (13), $\partial_x^2 I$ is the hessian of I (second order spatial derivative), where

$$\mathcal{G}(I) \stackrel{\text{def.}}{=} \alpha \star \nabla_x I + 2\partial_t \nabla_x I \quad \text{and} \quad \mathcal{H}(I) \stackrel{\text{def.}}{=} (\partial_x^2 I)$$

and $(\alpha, \beta, \Sigma_W)$ are defined in Proposition 4.

Proof. This follows by derivating in time the warping equation (12), denoting $y \stackrel{\text{def.}}{=} x + v_0 t$

$$\begin{aligned} \partial_t I_0(x, t) &= \partial_t I(y, t) + \langle \nabla I(y, t), v_0 \rangle, \\ \partial_t^2 I_0(x, t) &= \partial_t^2 I(y, t) + 2\langle \partial_t \nabla I(y, t), v_0 \rangle + \langle \partial_x^2 I(y, t)v_0, v_0 \rangle \end{aligned}$$

and plugging this into (13) after remarking that the distribution of $\frac{\partial W}{\partial t}(x, t)$ is the same as the distribution of $\frac{\partial W}{\partial t}(x - v_0 t, t)$. \square

Equation (19) is useful from a Bayesian modeling perspective, because, informally, it can be interpreted as the fact that the Gaussian distribution of MC as the following appealing form, for any function $\mathcal{I} : \mathbb{R}^2 \times \mathbb{R} \rightarrow \mathbb{R}$

$$\mathbb{P}_I(\mathcal{I}) = \frac{1}{Z_I} \exp(-\|\mathcal{D}(\mathcal{I}) + \langle \mathcal{G}(\mathcal{I}), v_0 \rangle + \langle \mathcal{H}(\mathcal{I})v_0, v_0 \rangle\|_{\Sigma_W^{-1}}^2)$$

where Z_I is a normalization constant which is independent of v_0 and

$$\|\mathcal{I}\|_{\Sigma_W^{-1}}^2 \stackrel{\text{def.}}{=} \langle \mathcal{I}, \mathcal{I} \rangle_{\Sigma_W^{-1}} \quad \text{and} \quad \langle \mathcal{I}_1, \mathcal{I}_2 \rangle_{\Sigma_W^{-1}} \stackrel{\text{def.}}{=} \int \int \frac{\hat{\mathcal{I}}_1(\xi, t) \hat{\mathcal{I}}_2(\xi, t)^*}{\hat{\sigma}_W^2(\xi)} d\xi dt$$

where $\hat{\sigma}_W$ is defined in (15).

This convenient formulation allows to re-write the MLE estimator of the horizontal speed v parameter of a MC as

$$\hat{v}^{\text{MLE}}(\mathcal{I}) \stackrel{\text{def.}}{=} \underset{v}{\operatorname{argmax}} \mathbb{P}_I(\mathcal{I}) \quad \text{where} \quad v_0 = (v, 0) \in \mathbb{R}^2$$

used to analyse psychophysical experiments as

$$\hat{v}^{\text{MLE}}(\mathcal{I}) = \underset{v}{\operatorname{argmin}} \|\mathcal{D}(\mathcal{I}) + v\langle\mathcal{G}(\mathcal{I}), (1, 0)\rangle + v^2\langle\mathcal{H}(\mathcal{I})(1, 0), (1, 0)\rangle\|_{\Sigma_w^{-1}}^2 \quad (20)$$

where we used the fact that the normalizing constant Z_I is independent of v_0 . Expanding the squares shows that (20) is the optimization of a fourth order polynomial, whose solution can be computed in closed form as one of the roots of the derivative of this polynomial, which is hence a third order polynomial.

C.2 MLE Modeling of the Likelihood

In our paper, following several previous works such as [13, 12], we assumed the existence of an internal representation parameter m , which was assumed to be a scalar, with a Gaussian distribution conditioned on (v, z) . We explore here the possibility that this internal representation could be directly obtained from the stimuli by the usage by the observer of an “optimal” speed detector (an MLE estimate).

Denoting $I_{v,z}$ a MC, which is a random Gaussian field of power spectrum (11), with central speeds $v_0 = (v, 0)$ and central spacial frequency z (the other parameters being fixed as explained in the experimental section of the paper), this means that we consider the internal representation as being the following scalar random variable

$$M_{v,z} \stackrel{\text{def.}}{=} \hat{v}_z^{\text{MLE}}(I_{v,z}) \quad \text{where} \quad \hat{v}_z^{\text{MLE}}(\mathcal{I}) \stackrel{\text{def.}}{=} \underset{v}{\operatorname{argmax}} \mathbb{P}_{M|V,Z}(\mathcal{I}|v, z), \quad (21)$$

As detailed in (20) it can be efficiently computed numerically.

As shown in Figure 6(a), we observed that $M_{v,z}$ is well approximated by a Gaussian random variable. Its mean is nearly constant and very close to v , and Figure 6(b) shows the evolution of its variance. Our main finding is that this optimal estimation model (using an MLE) is not consistent with the experimental finding because the estimated standard deviations of observers don’t show a decreasing behavior as in Figure 6(b).

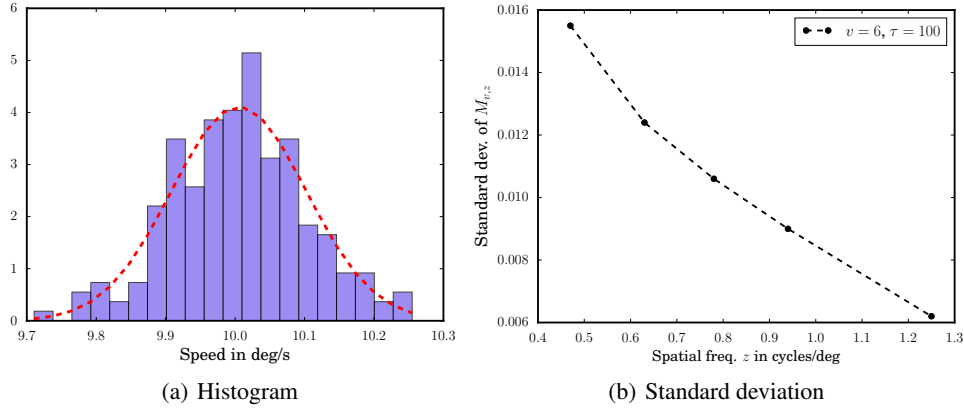


Figure 6: Estimates of $M_{v,z}$ defined by (21) and its standard deviation as a function of z .

C.3 Prior slope and Likelihood width fitting

In Section 3 we use equations

$$\sigma_z^2 = \lambda_{z,z^*}^2 - \frac{1}{2}\lambda_{z^*,z^*}^2 \quad \text{and} \quad a_z = a_{z^*} \frac{\sigma_{z^*}^2}{\sigma_z^2} - \frac{\mu_{z,z^*}}{\sigma_z^2}$$

to determine a_z and σ_z . The slopes a_z are noisy due to the quotient $\frac{\sigma_{z^*}^2}{\sigma_z^2}$ therefore we only show some of the best fit in Figure 7 when the approximation σ_z^2 constant holds.

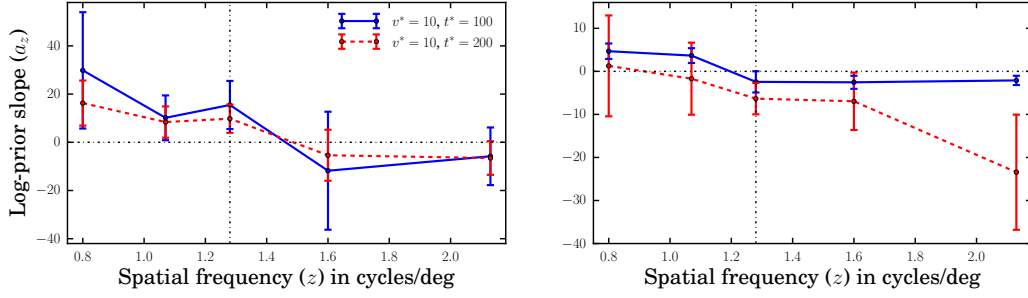


Figure 7: Example of decreasing a_z . The unknown a_{z^*} chosen so that $\sum_z a_z^2$ is minimum.

D Proofs

D.1 Proof of Proposition 2

We recall the expression of the covariance

$$\forall (x, t) \in \mathbb{R}^3, \quad \gamma(x, t) = \int \int_{\mathbb{R}^2} c_g(\varphi_a(x - \nu t)) \mathbb{P}_V(\nu) \mathbb{P}_A(a) d\nu da \quad (22)$$

We denote $(\theta, \varphi, z, r) \in \Gamma = [-\pi, \pi)^2 \times \mathbb{R}_+^2$ the set of parameters. According to Proposition 1, the covariance of I is γ defined by (22). Denoting $h(x, t) = c_g(z R_\theta(x - \nu t))$, one has, in the sense of distributions (taking the Fourier transform with respect to (x, t))

$$\hat{h}(\xi, \tau) = z^{-2} \hat{g}(z^{-1} R_\theta(\xi))^2 \delta_{\mathcal{Q}}(\nu) \quad \text{where} \quad \mathcal{Q} = \{\nu \in \mathbb{R}^2 ; \tau + \langle \xi, \nu \rangle = 0\}.$$

Taking the Fourier transform of (22) and using this computation, one has

$$\hat{\gamma}(\xi, \tau) = \int_{\Gamma} \frac{1}{z^2} |\hat{g}(z^{-1} R_\theta(\xi))|^2 \delta_{\mathcal{Q}}(v_0 + r(\cos(\varphi), \sin(\varphi))) \mathbb{P}_\Theta(\theta) \mathbb{P}_Z(z) \mathbb{P}_{\|V - v_0\|}(r) d\theta dz dr d\varphi.$$

In the special case of g being a grating, i.e. $|\hat{g}|^2 = \delta_{\xi_0}$, one has in the sense of distributions

$$z^{-2} |\hat{g}(z^{-1} R_\theta(\xi))|^2 = \delta_{\mathcal{B}}(\theta, z) \quad \text{where} \quad \mathcal{B} = \{(\theta, z) ; z^{-1} R_\theta(\xi) = \xi_0\}.$$

Observing that $\delta_{\mathcal{Q}}(\nu) \delta_{\mathcal{B}}(\theta, z) = \delta_{\mathcal{C}}(\theta, z, r)$ where

$$\mathcal{C} = \left\{ (\theta, z, r) ; z = \|\xi\|, \theta = \angle \xi, r = -\frac{\tau}{\|\xi\| \cos(\angle \xi - \varphi)} - \frac{\|v_0\| \cos(\angle \xi - \angle v_0)}{\cos(\angle \xi - \varphi)} \right\}$$

one obtains the desired formula.

D.2 Proof of Proposition 3

One has the closed form expression for the MAP estimator

$$\hat{v}_z(m) = m - a_z \sigma_z^2,$$

and hence, denoting $\mathcal{N}(\mu, \sigma^2)$ the Gaussian distribution of mean μ and variance σ^2 ,

$$\hat{v}_z(M_{v,z}) \sim \mathcal{N}(v - a_z \sigma_z^2, \sigma_z^2)$$

where \sim means equality of distributions. One thus has

$$\hat{v}_{z^*}(M_{v,z^*}) - \hat{v}_z(M_{v^*,z}) \sim \mathcal{N}(v - v^* - a_{z^*} \sigma_{z^*}^2 + a_z \sigma_z^2, \sigma_{z^*}^2 + \sigma_z^2),$$

which leads to the results by taking expectation.

References

- [1] Adelson, E. H. and Bergen, J. R. (1985). Spatiotemporal energy models for the perception of motion. *Journal of Optical Society of America, A.*, 2(2):284–99.

- [2] Dong, D. (2010). Maximizing causal information of natural scenes in motion. In Ilg, U. J. and Masson, G. S., editors, *Dynamics of Visual Motion Processing*, pages 261–282. Springer US.
- [3] Doretto, G., Chiuso, A., Wu, Y. N., and Soatto, S. (2003). Dynamic textures. *International Journal of Computer Vision*, 51(2):91–109.
- [4] Field, D. J. (1987). Relations between the statistics of natural images and the response properties of cortical cells. *J. Opt. Soc. Am. A*, 4(12):2379–2394.
- [5] Galerne, B. (2011). *Stochastic image models and texture synthesis*. PhD thesis, ENS de Cachan.
- [6] Galerne, B., Gousseau, Y., and Morel, J. M. (2011). Micro-Texture synthesis by phase randomization. *Image Processing On Line*, 1.
- [7] Gregory, R. L. (1980). Perceptions as hypotheses. *Philosophical Transactions of the Royal Society B: Biological Sciences*, 290(1038):181–197.
- [8] Jogan, M. and Stocker, A. A. (2015). Signal integration in human visual speed perception. *The Journal of Neuroscience*, 35(25):9381–9390.
- [9] Nestares, O., Fleet, D., and Heeger, D. (2000). Likelihood functions and confidence bounds for total-least-squares problems. In *IEEE Conference on Computer Vision and Pattern Recognition. CVPR 2000*, volume 1, pages 523–530. IEEE Comput. Soc.
- [10] Sanz-Leon, P., Vanzetta, I., Masson, G. S., and Perrinet, L. U. (2012). Motion clouds: model-based stimulus synthesis of natural-like random textures for the study of motion perception. *Journal of Neurophysiology*, 107(11):3217–3226.
- [11] Simoncini, C., Perrinet, L. U., Montagnini, A., Mamassian, P., and Masson, G. S. (2012). More is not always better: adaptive gain control explains dissociation between perception and action. *Nature Neurosci*, 15(11):1596–1603.
- [12] Sotiropoulos, G., Seitz, A. R., and Seriès, P. (2014). Contrast dependency and prior expectations in human speed perception. *Vision Research*, 97(0):16 – 23.
- [13] Stocker, A. A. and Simoncelli, E. P. (2006). Noise characteristics and prior expectations in human visual speed perception. *Nature Neuroscience*, 9(4):578–585.
- [14] Unser, M. and Tafti, P. (2014). *An Introduction to Sparse Stochastic Processes*. Cambridge University Press, Cambridge, UK. 367 p.
- [15] Unser, M., Tafti, P. D., Amini, A., and Kirshner, H. (2014). A unified formulation of gaussian versus sparse stochastic processes - part II: Discrete-Domain theory. *IEEE Transactions on Information Theory*, 60(5):3036–3051.
- [16] Wei, L. Y., Lefebvre, S., Kwatra, V., and Turk, G. (2009). State of the art in example-based texture synthesis. In *Eurographics 2009, State of the Art Report, EG-STAR*. Eurographics Association.
- [17] Wei, X.-X. and Stocker, A. A. (2012). Efficient coding provides a direct link between prior and likelihood in perceptual bayesian inference. In Bartlett, P. L., Pereira, F. C. N., Burges, C. J. C., Bottou, L., and Weinberger, K. Q., editors, *NIPS*, pages 1313–1321.
- [18] Weiss, Y. and Fleet, D. J. (2001). Velocity likelihoods in biological and machine vision. In *In Probabilistic Models of the Brain: Perception and Neural Function*, pages 81–100.
- [19] Weiss, Y., Simoncelli, E. P., and Adelson, E. H. (2002). Motion illusions as optimal percepts. *Nature Neuroscience*, 5(6):598–604.
- [20] Xia, G. S., Ferradans, S., Peyré, G., and Aujol, J. F. (2014). Synthesizing and mixing stationary gaussian texture models. *SIAM Journal on Imaging Sciences*, 7(1):476–508.
- [21] Young, R. A. and Lesperance, R. M. (2001). The gaussian derivative model for spatial-temporal vision: II. cortical data. *Spatial vision*, 14(3):321–390.